Supplementary Information for

Genome-wide transcriptomic analysis of microglia reveals impaired responses in aged mice after cerebral ischemia

Ligen Shi, Marcelo Rocha, Wenting Zhang, Ming Jiang, Sicheng Li, Qing Ye, Sulaiman H. Hassan, Liqiang Liu, Maya N. Adair, Jing Xu, Jianhua Luo, Xiaoming Hu, Lawrence R. Wechsler, Jun Chen, and Yejie Shi

Corresponding author: Yejie Shi
Email: y.shi@pitt.edu

This PDF file includes:

Supplementary Methods
Supplementary Figures 1-6
Supplementary Tables 1-7
Supplementary References

Supplementary Methods

Choose of sample size

Sample sizes for the bulk RNA sequencing (RNA-seq) experiments were determined based on what is commonly used for this technique in the literature. The number of animals required for the *in vivo* studies was determined by power analysis based on our experience with the murine distal middle cerebral artery occlusion (dMCAO) model. To detect a 30% difference in infarct volume between two groups with 80% power at an α value of 0.05 (two-tailed), approximately 6 mice per group were needed. For flow cytometry and immunohistochemistry, 4-6 samples were required for 80% power (β=0.8, α=0.05) to detect a 25% change after dMCAO.

Animals

Young adult male C57BL/6J mice (10 weeks old) were purchased from the Jackson Laboratory. Aged male C57BL/6 mice (18 months old) were obtained from the National Institute on Aging (NIA) aged mouse colony at Charles River Laboratories. Mice were housed in a temperature and humidity-controlled animal facility with a 12-h light/dark cycle. Food and water were available *ad libitum*. All animal procedures were approved by the University of Pittsburgh Institutional Animal Care and Use Committee, performed in accordance with the *Guide for the Care and Use of Laboratory Animals*,[1] and reported following the ARRIVE guidelines.[2] All efforts were made to minimize animal suffering and the number of animals used.

Permanent focal cerebral ischemia

Focal cerebral ischemia was induced in young adult and aged mice by permanent occlusion of the left distal middle cerebral artery (MCA) and left common carotid artery (CCA), as described previously.[3,4] We refer to this model as dMCAO. Briefly, a skin incision was made at the midline of the neck, and the left CCA was exposed and ligated. A craniotomy was performed between the left eye and the ear, to expose the conjunction of the rhinal fissure and MCA. The distal branch of the left MCA was then occluded with low intensity bipolar electrocautery (Codman & Shurtleff Inc.) at the immediate lateral part of the rhinal fissure. Both the rectal temperature and the left temporalis muscle temperature were maintained at 37.0±0.5°C during surgery with a temperature-controlled heating pad and a heat lamp. Mean arterial blood pressure was monitored during surgery by a tail cuff. Cortical cerebral blood flow (CBF) was monitored using two-dimensional laser speckle techniques (PeriCam PSI HR System, Perimed) according to the manufacturer's instructions, as before.[5] Failure to reduce cortical CBF to 30% or less of baseline levels or premature death before the targeted endpoint led to subject exclusion. According to the experimental records of our laboratory, the exclusion rate was less than 10% in approximately 500 mice in the last 5 years. Sham-operated animals underwent the same anesthesia and surgical procedures, with the exception of occlusion of the CCA and MCA.

Experimental procedures were performed following criteria derived from *Stroke Therapy Academic Industry Roundtable* (STAIR) group guidelines for preclinical evaluation of stroke therapeutics.[6] Accordingly, experimental group assignments were randomized with a lottery-drawing box, and surgeries and all outcome assessments were performed by investigators blinded to experimental group assignments.

Flow cytometry and fluorescence-activated cell sorting (FACS)

Single-cell suspensions were prepared from the mouse brain, as described previously.[7,8] Briefly, mice were deeply anesthetized and transcardially perfused with 0.9% NaCl. The ipsilesional brain hemisphere was harvested, and cell suspensions were prepared using the Neural Tissue Dissociation Kit and gentleMACS Octo Dissociator with Heaters (Miltenyi Biotec) according to the manufacturer's instructions. Suspensions were passed through a 70 μm cell strainer and fractionated on a 30% and 70% Percoll (GE Healthcare BioSciences) gradient at 500 *g* for 30 min to remove myelin and cell debris. Mononuclear cells at the interface were collected and washed with FACS buffer (1% PS antibiotic, 2 nM EDTA, 2% FBS in HBSS buffer). Cells were then resuspended at 1×10^6 cells per mL, and stained with the following fluorophore-conjugated antibodies and the appropriate isotype controls: PerCP-Cy5.5 labeled anti-CD45 (eBioscience 45-0451-82), BV605 labeled anti-CD11b (BD 563015), FITC labeled anti-Ly6G (eBioscience 11-9668-82), BV421 labeled anti-CD11c (BD 562782), eFluor450 labeled anti-CD45 (eBioscience 48-0451-82), APC-eFluor 780 labeled anti-CD11b (eBioscience 47-0112-82), PerCP-Cyanine5.5 labeled anti-CD11c (eBioscience 45-0114-82), BUV395 labeled anti-Ly6G (BD 563978), BV605 labeled anti-Ly6C (BD 563011), APC labeled anti-CD3 (eBioscience 17-0032-82), BUV395 labeled anti-CD19 (BD 563557), PE labeled anti-CD4 (eBioscience 12-0041-82), and PerCP-Cyanine5.5 labeled anti-CD8a (eBioscience 45-0081-82).

Flow cytometry was performed using an LSR II flow cytometer and FACS Diva software (BD Biosciences) or a Cytek Aurora flow cytometer and SpectroFlo software. Flow cytometry data were further analyzed using the FlowJo software (FlowJo, LLC) to quantify positively stained cells. FACS was performed using an FACS Aria I sorter and FACS Diva software (BD Biosciences). Microglia were gated as $CD11c^{-}Ly6G^{-}CD11b^{+}CD45^{low}$ and sorted for bulk RNA-seq. Each sample was pooled from 5 mouse brains to obtain enough cells.

RNA sequencing

RNA extraction, library preparation, and sequencing were performed at the next-generation sequencing core facility at the University of California at Los Angeles. Total RNA was extracted from FACS-sorted microglia using RNeasy Plus micro/mini kits (Qiagen), according to the manufacturer's instructions. RNA quality was assessed using an Agilent Bioanalyzer. All RNA used had an RNA Integrity Number (RIN) larger than 9.2. Libraries for RNA-seq were prepared from 300 ng of total RNA with the Clonetech SMARTer Stranded Total RNA-Seq (Pico) Kit. The

workflow consisted of first-strand synthesis, template switching, adaptor ligation, cleavage of ribosomal cDNA and PCR amplification. Different adaptors were used for multiplexing samples in one lane. Sequencing was performed on an Illumina Hiseq3000 sequencing system for a single-end read 50-bp run. Data quality checks were performed on Illumina Sequencing Analysis Viewer. Demultiplexing was performed with the Illumina bcl2fastq2 (v2.17) program.

Bioinformatics analysis of RNA-seq data

Preprocessing.

Raw data from high-throughput sequencing were stored in FASTQ format files, which contained reads sequence and corresponding base quality. After cleaning up adapter contamination and low-quality regions, we used TopHat2[9] to align trimmed reads to mouse reference genome sequences (mm10) and transcript annotation from GENCODE[10] (v19). We then applied Cufflinks[11] (v2.2.1) to estimate gene and isoform abundance. The estimation of abundance was in Fragments Per Kilobase of transcript per Million mapped reads (FPKM) format. In addition, we applied HTSeq[12] (v0.11.2) to quantify gene expression by the numbers of read counts.

Differential expression analysis.

We used R/Bioconductor[13] with the *edgeR* package[14] to normalize the read counts and perform differential expression analysis. Differentially expressed genes (DEGs) were defined as genes with a fold change > 2 or < -2, and with a false discovery rate (FDR) < 0.05. Heatmaps were generated using the R package *pheatmap*.

Functional enrichment analysis.

Functional enrichment analysis was performed with an online tool *Metascape* (http://metascape.org).[15] All genes in the mouse genome were used as the enrichment background. *Metascape* returns a list of significantly overrepresented (P < 0.01) ontology terms with a minimum count of 3, and an enrichment factor (the ratio between the observed counts and the counts expected by chance) larger than 1.5. Terms were grouped into clusters based on their membership similarities, and rendered as a network plot where terms with a similarity > 0.3 were connected by edges. Alternatively, enrichment data were visualized as bubble plots or Circos plots using the R package *GOplot*.[16] The activation z-score of each ontology term was calculated by *GOplot* as (number of upregulated genes – number of downregulated genes) / square root of the number of genes assigned to a term. A term was predicted to be significantly activated/increased with a z-score > 2 and a P-value < 0.01, and was predicted to be significantly inhibited/decreased with a z-score < -2 and a P-value < 0.01.

Ingenuity Pathway Analysis (IPA).

We submitted the DEGs identified by *edgeR* to IPA for pathway analysis using the Ingenuity Knowledge Base (Qiagen Bioinformatics).[17] The fold change and FDR of each gene were used to perform the core analysis. Diseases and functions were considered significantly enriched with a

P-value of overlap < 0.01 and an activation z-score > 2 (predicted to be activated) or < -2 (predicted to be inhibited).

Immunohistochemistry and data analyses

Mice were deeply anesthetized and transcardially perfused with 0.9% NaCl, followed by 4% paraformaldehyde in PBS. Brains were harvested and cryoprotected in 30% sucrose in PBS, and frozen serial coronal brain sections (25-μm thick) were prepared on a sliding microtome (Microm HM 450; Thermo Scientific). Sections were blocked with 5% donkey serum in PBS for 1 h, followed by overnight incubation (4°C) with the following primary antibodies: anti-Clec7a (R&D Systems AF1756), anti-microtubule-associated protein 2 (MAP2; Santa Cruz Biotechnology sc-20172), anti-NeuN (Millipore MAB377), anti-APC (Calbiochem OP80), anti-glial fibrillary acidic protein (GFAP; Invitrogen 13-0300), anti-Tmem119 (Abcam ab209064), and anti-Iba1 (Wako 019-19741). After washing, sections were incubated for 1 h at 20°C with donkey secondary antibodies conjugated with DyLight 488 or Cy3 fluorophores (1:1000, Jackson ImmunoResearch Laboratories). Alternate sections from each experimental condition were incubated in all solutions except the primary antibodies to assess nonspecific secondary antibody staining. Sections were then mounted and coverslipped with Fluoromount-G containing DAPI (Southern Biotech). Fluorescence images were captured with an inverted Nikon Diaphot-300 fluorescence microscope equipped with a SPOT RT slider camera and Meta Series Software 5.0 (Molecular Devices), or with an Olympus Fluoview FV1000 confocal microscope and FV10-ASW 2.0 software.

Infarct volume was measured using ImageJ on six equally spaced sections encompassing the MCA territory immunostained for MAP2. Infarct volume was calculated as the volume of the MAP2-immunopositive contralesional hemisphere minus that of the ipsilesional side.

Imaris 3-D rendering and quantification

The image-processing software Imaris (Bitplane; v9.3) was used to reconstruct three-dimensional images of immunofluorescence signal. Image stacks obtained by confocal microscopy were imported into Imaris, and the *surface* module was used to generate 3D structures of each color channel, as described previously.[18] Briefly, a region of interest was selected, and the absolute intensity of each source channel was used for reconstruction. Smoothing was set at 0.400 μm for all channels and images. A threshold was set to differentiate the target signal from background, and the same threshold value was used for all groups. Non-specific signals were then removed, and the 3D-rendered images were constructed. All images were processed with the same adjustments and parameters. The surface contact area among various types of cells was manually reconstructed and calculated using a MATLAB plugin *surface to surface contact* in Imaris based on the 3D-rendered images. To measure the polarity of Tmem119$^+$ microglia, the processes of each Tmem119$^+$ cell were traced by the *filament* module in Imaris in a semi-automated manner. Briefly, the center of the cell body and the end of each process were manually defined, and the

processes were then automatically traced by the *auto-path* function according to the intensity of Tmem119 immunofluorescence. The polarity of each cell with regard to the infarct core was determined in a polar coordinate system, where the direction from cell body to infarct core was defined as 135°. The upper left quadrant (from 90° to 180°) in the polar coordinate system was defined as the target quadrant, and the number of processes in the target quadrant was counted and expressed as percentage of total number of processes in all four quadrants.

Statistical analysis

High-throughput sequencing data were analyzed, as described above. Other datasets are presented as mean ± standard deviation (SD). Individual data points are plotted where applicable. Statistical comparison of the means between two groups was accomplished by the Student's *t* test or the Mann-Whitney *U* test (both two-tailed). Differences in means among multiple groups were analyzed using one-way ANOVA, followed by the Bonferroni/Dunn *post hoc* correction. The analyses were performed using Prism 8 (GraphPad). A *P* value equal to or less than 0.05 was deemed statistically significant. All statistics are summarized in Supplementary Table 1.

Data availability

All RNA-seq data are deposited in the Gene Expression Omnibus database at the National Center for Biotechnology Information (accession number GSE145265). Other data that support the findings of this study are available from the corresponding authors upon request. There are no restrictions on data availability.

Supplementary Figures

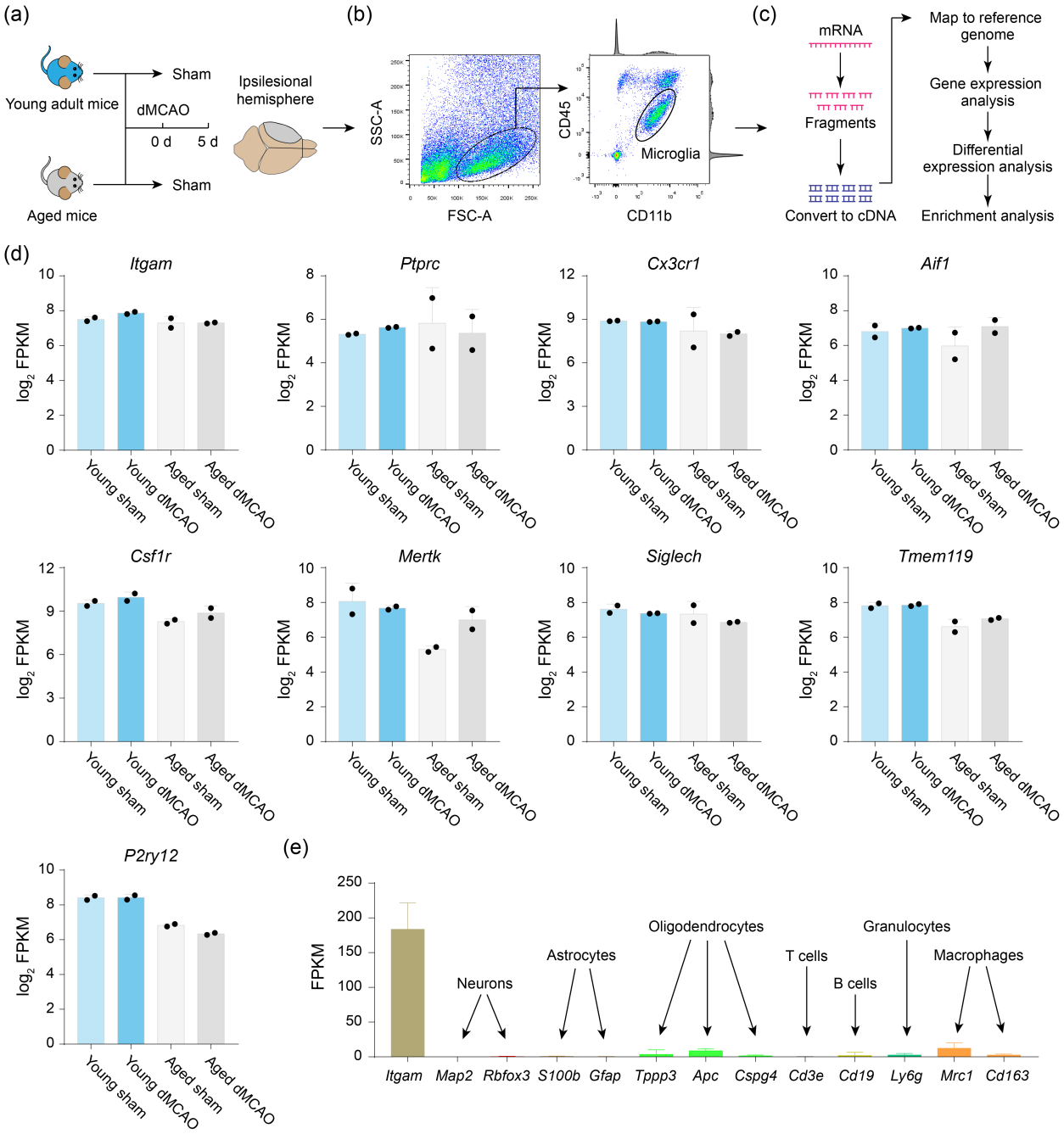

Supplementary Figure 1. RNA sequencing profiling of microglia in the mouse brain.

(a-c) Experimental design. Young adult mice (10 weeks old) and aged mice (18 months old) were subjected to focal cerebral ischemia induced by dMCAO or sham operation. Five days after dMCAO or after sham, microglia ($CD11b^{+}CD45^{low}$ cells) were sorted from the ipsilesional brain hemisphere by FACS (b) and subjected to bulk RNA-seq. (c) The workflow of RNA-seq and data

analysis. (d) RNA-seq expression profiles of established microglia marker genes in FACS-isolated cells. (e) RNA-seq expression profiles of established marker genes for neurons, astrocytes, oligodendrocytes, T cells, B cells, granulocytes and macrophages with comparison to the microglial marker *Itgam* (encoding CD11b) in FACS-sorted cells. n=2 biological replicates per group, and each biological replicate was pooled from 5 mouse brains.

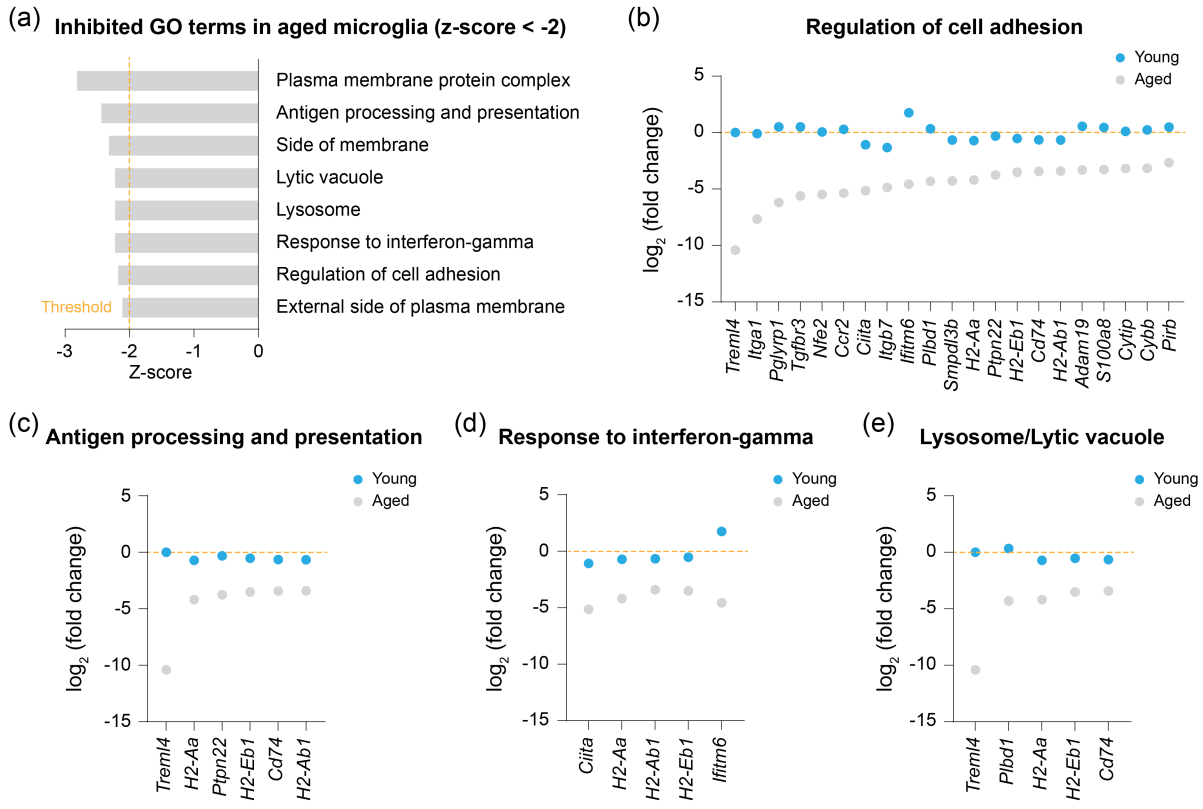

Supplementary Figure 2. Inhibited biological functions in aged microglia after dMCAO (related to Figure 3).

(a) Gene ontology (GO) enrichment analysis was performed on DEGs in aged microglia from the dMCAO brain versus sham brain by *Metascape*. The activation z-score of each GO term was calculated by *GOplot*. Shown are GO terms that were predicted to be strongly inhibited (z-score < -2, $P < 0.01$) in aged microglia after dMCAO. (b-e) Expression profiles of downregulated DEGs in aged microglia (fold change < -2, FDR < 0.05) under the GO terms *regulation of cell adhesion* (b), *antigen processing and presentation* (c), *response to interferon-gamma* (d), and *lysosome/lytic vacuole* (e) are shown with comparison to their expression in young microglia. None of these genes was differentially expressed in young microglia (FDR > 0.05).

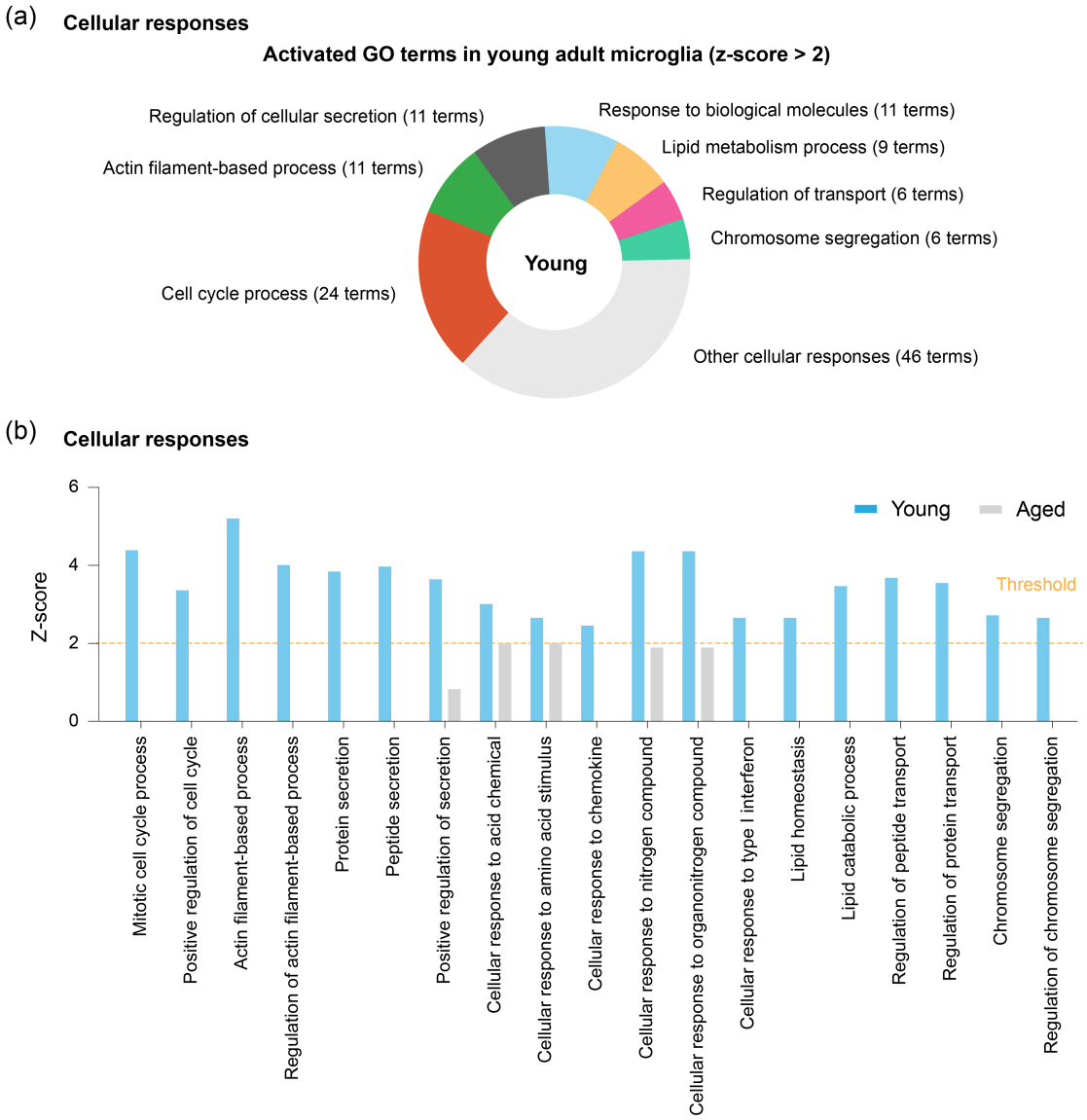

Supplementary Figure 3. Aged microglia demonstrate impaired cellular responses compared to young microglia after ischemic stroke (related to Figure 3).

GO enrichment analysis was performed by *Metascape* on all dMCAO-induced DEGs in young and aged microglia. (a) Shown are the numbers of significantly overrepresented ($P < 0.01$) GO terms with an activation z-score > 2 in the *cellular responses* functional cluster in young microglia. A total of 124 GO terms in *cellular responses* (see Figure 3(c)) were classified into 8 sub-categories. (b) Shown are the activation z-scores of representative biological functions related to cellular responses that were predicted to be strongly activated (z-score > 2) in young microglia in response to dMCAO. Only 5 of these functions were significantly overrepresented ($P < 0.01$) in aged microglia, and none of them was predicted to be significantly activated in aged microglia (0 < z-score < 2).

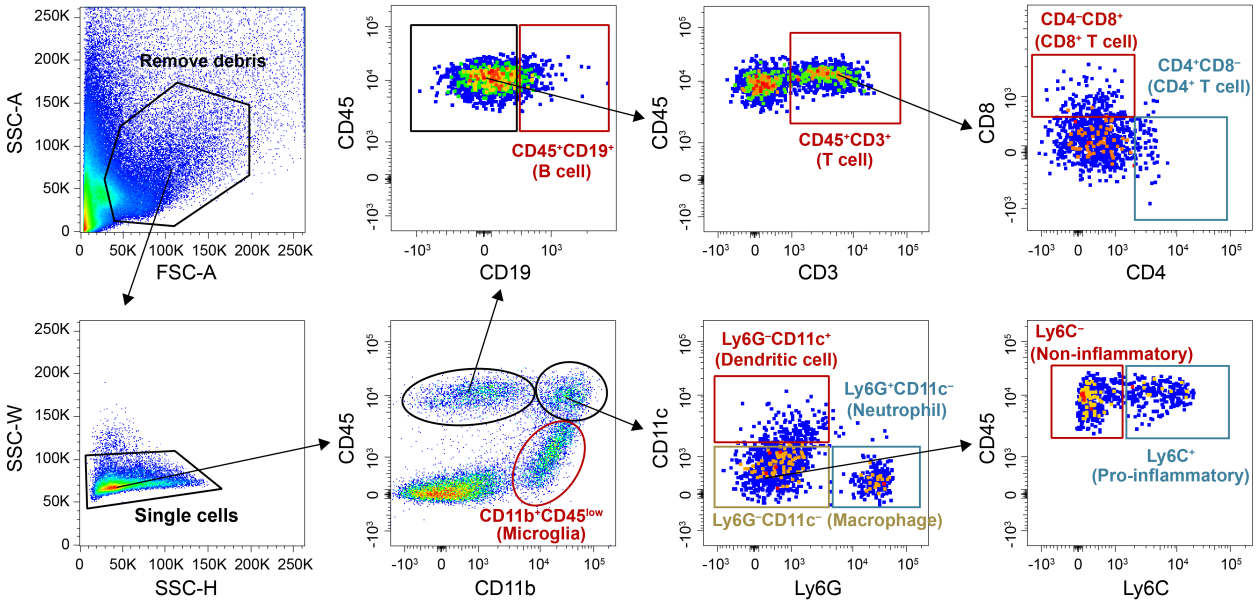

Supplementary Figure 4. Gating strategy for flow cytometry of brain cells after dMCAO (related to Figure 4).

Young adult mice and aged mice were subjected to dMCAO. Five days after dMCAO, cell suspensions were prepared from the ipsilesional and non-injured contralesional brain hemispheres of each mouse, and flow cytometry was performed to quantify the numbers of various immune cells in the brain as follows: microglia ($CD11b^{+}CD45^{low}$), B cells ($CD45^{+}CD19^{+}$), T cells ($CD45^{+}CD3^{+}$), neutrophil ($CD45^{+}Ly6G^{+}CD11c^{-}$), dendritic cells ($CD45^{+}Ly6G^{-}CD11c^{+}$), and macrophages ($CD11b^{+}CD45^{high}Ly6G^{-}$). Macrophages were further gated into pro-inflammatory macrophages ($CD11b^{+}CD45^{high}Ly6C^{+}$) and non-inflammatory macrophages ($CD11b^{+}CD45^{high}$ $Ly6C^{-}$) according to the expression level of Ly6C.

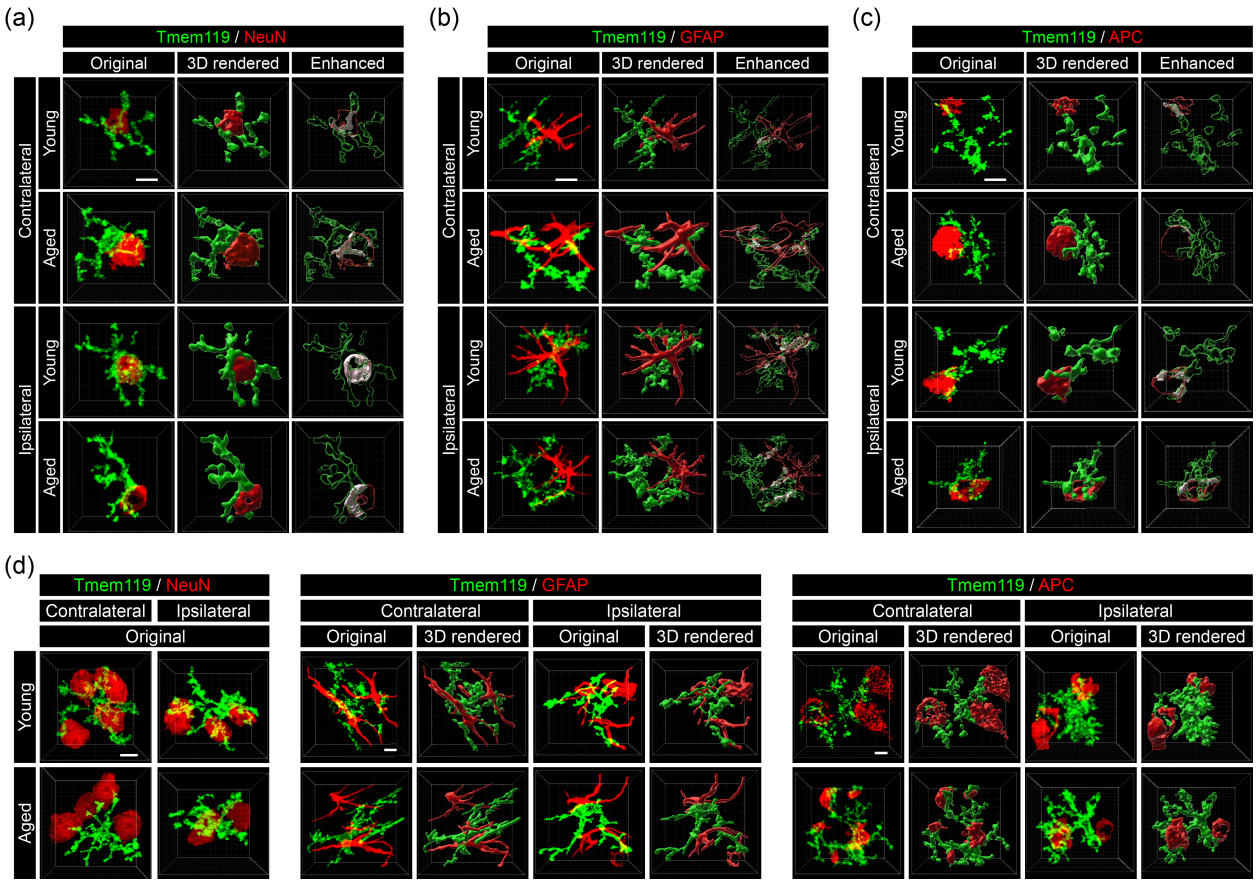

Supplementary Figure 5. Aged microglia demonstrate less interaction with neurons in the post-stroke brain (related to Figure 7).

Young adult and aged mice were subjected to dMCAO. Five days after dMCAO, double-label immunofluorescence staining was performed to examine the interaction between microglia and other types of brain cells in the ipsilesional peri-infarct region and the corresponding region in the non-injured contralateral hemisphere. (a-c) Original and Imaris-processed images showing the cell-cell contact areas between Tmem119^{+} microglia and NeuN^{+} neurons (a), GFAP^{+} astrocytes (b), and APC^{+} oligodendrocytes (c), related to Figure 7(a) – 7(c). The original images from confocal microscopy (1st columns) were 3D surface-rendered by Imaris (2nd columns), and the cell-cell contact areas were enhanced in white color (3rd columns). (d) Original images taken by confocal microscopy and 3D surface-rendered images showing the interaction between Tmem119^{+} microglia and NeuN^{+} neurons (left panel), GFAP^{+} astrocytes (middle panel), and APC^{+} oligodendrocytes (right panel), related to Figure 7(e). Scale bars: 5 µm.

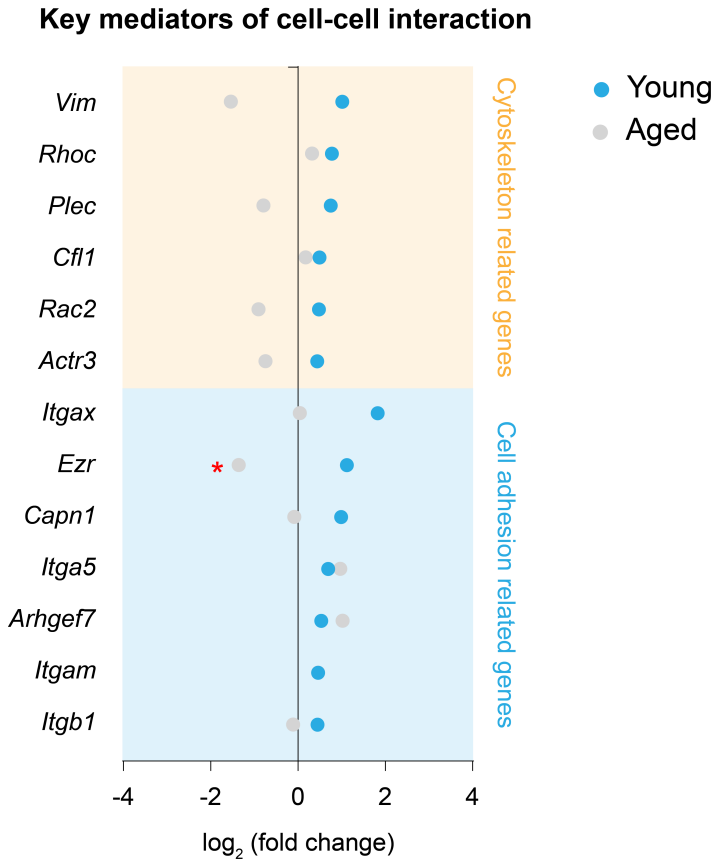

Supplementary Figure 6. Aged microglia harbor less genomic changes favoring cell-cell interactions than young microglia after ischemic stroke (related to Figure 7).

Shown are the expression profiles of a panel of cytoskeleton and cell adhesion regulators that were differentially expressed (FDR < 0.05) in young microglia after dMCAO with comparison to their expression in aged microglia. **P*<0.05 aged dMCAO vs. aged sham.

Supplementary Tables

Supplementary Table 1. Statistics reporting.

FIGURE	n	DATA STRUCTURE	TEST USED	STATISTIC	P VALUE
1(b) (percentage)	6 mice (young) 6 mice (aged)	Non-normal distribution	Mann-Whitney *U* test	$U = 0$	aged-young = 0.0022
1(b) (ischemic area)	6 mice (young) 6 mice (aged)	Normal distribution	One-way ANOVA; Bonferroni *post hoc*	$F_{(3, 20)} = 10.72$	ANOVA P=0.0002 aged-young = 0.0179 (core) aged-young > 0.9999 (penumbra)
1(d)	6 mice (young 3d) 6 mice (aged 3d) 6 mice (young 5d) 6 mice (aged 5d)	Normal distribution	*t* test (two-tailed)	$t_{(10)} = 2.300$ (3d) $t_{(10)} = 2.417$ (5d)	aged-young = 0.0443 (3d) aged-young = 0.0363 (5d)
1(g)	8 mice (young) 8 mice (aged)	Normal distribution	One-way ANOVA; Bonferroni *post hoc*	$F_{(3, 28)} = 23.33$	ANOVA P<0.0001 Young IL-CL<0.0001 Aged IL-CL<0.0001 CL aged-young>0.9999 IL aged-young>0.9999
1(h)	16 cells (young) 16 cells (aged) from 4 mice per group	Normal distribution	One-way ANOVA; Bonferroni *post hoc*	$F_{(3, 60)} = 20.89$	ANOVA P<0.0001 Young IL-CL=0.0001 Aged IL-CL<0.0001 CL aged-young=0.3695 IL aged-young=0.0453
4(d) (B cell)	5 mice (young) 5 mice (aged)	Normal distribution	One-way ANOVA; Bonferroni *post hoc*	$F_{(3, 16)} = 136.5$	ANOVA P<0.0001 Young IL-CL<0.0001 Aged IL-CL<0.0001 CL aged-young>0.9999 IL aged-young=0.0015
4(d) ($CD3^+$ T cell)	5 mice (young) 5 mice (aged)	Normal distribution	One-way ANOVA; Bonferroni *post hoc*	$F_{(3, 16)} = 96.30$	ANOVA P<0.0001 Young IL-CL<0.0001 Aged IL-CL<0.0001 CL aged-young>0.9999 IL aged-young<0.0001
4(d) ($CD4^+$ T cell)	5 mice (young) 5 mice (aged)	Normal distribution	One-way ANOVA; Bonferroni *post hoc*	$F_{(3, 16)} = 32.39$	ANOVA P<0.0001 Young IL-CL<0.0001 Aged IL-CL<0.0001 CL aged-young>0.9999 IL aged-young=0.0044
4(d) ($CD8^+$ T cell)	5 mice (young) 5 mice (aged)	Normal distribution	One-way ANOVA; Bonferroni *post hoc*	$F_{(3, 16)} = 67.91$	ANOVA P<0.0001 Young IL-CL<0.0001 Aged IL-CL=0.0060 CL aged-young>0.9999 IL aged-young=0.0018
4(d) (neutrophil)	5 mice (young) 5 mice (aged)	Normal distribution	One-way ANOVA; Bonferroni *post hoc*	$F_{(3, 16)} = 10.41$	ANOVA P=0.0005 Young IL-CL=0.0145 Aged IL-CL>0.9999 CL aged-young=0.9142 IL aged-young=0.0023
4(d) (dendritic cell)	5 mice (young) 5 mice (aged)	Non-normal distribution	One-way ANOVA on ranks (Kruskal-Wallis test); Dunn *post hoc*	$H_{(3)} = 14.63$	ANOVA P=0.0022 Young IL-CL=0.0166 Aged IL-CL=0.1121 CL aged-young>0.9999 IL aged-young>0.9999

4(d) (microglia)	5 mice (young) 5 mice (aged)	Normal distribution	One-way ANOVA; Bonferroni *post hoc*	$F_{(3, 16)} = 77.79$	ANOVA P<0.0001 Young IL-CL<0.0001 Aged IL-CL<0.0001 CL aged-young=0.5239 IL aged-young=0.6501
4(d) (macrophage)	5 mice (young) 5 mice (aged)	Normal distribution	One-way ANOVA; Bonferroni *post hoc*	$F_{(3, 16)} = 180.4$	ANOVA P<0.0001 Young IL-CL<0.0001 Aged IL-CL<0.0001 CL aged-young>0.9999 IL aged-young<0.0001
4(e) ($Ly6C^+$ macrophage)	5 mice (young) 5 mice (aged)	Normal distribution	One-way ANOVA; Bonferroni *post hoc*	$F_{(3, 16)} = 104.0$	ANOVA P<0.0001 Young IL-CL<0.0001 Aged IL-CL=0.0001 CL aged-young>0.9999 IL aged-young<0.0001
4(e) ($Ly6C^-$ macrophage)	5 mice (young) 5 mice (aged)	Normal distribution	One-way ANOVA; Bonferroni *post hoc*	$F_{(3, 16)} = 95.83$	ANOVA P<0.0001 Young IL-CL<0.0001 Aged IL-CL<0.0001 CL aged-young>0.9999 IL aged-young=0.0015
6(f)	5 mice (young) 3 mice (aged)	Normal distribution	*t* test (two-tailed)	$t_{(6)} = 3.147$	Aged-young=0.0199
7(d) (neuron)	12 cells (young) 12 cells (aged) from 4 mice per group	Normal distribution	One-way ANOVA; Bonferroni *post hoc*	$F_{(3, 44)} = 61.53$	ANOVA P<0.0001 Young IL-CL<0.0001 Aged IL-CL<0.0001 CL aged-young>0.9999 IL aged-young<0.0001
7(d) (astrocyte)	12 cells (young) 12 cells (aged) from 4 mice per group	Normal distribution	One-way ANOVA; Bonferroni *post hoc*	$F_{(3, 44)} = 11.08$	ANOVA P<0.0001 Young IL-CL=0.0008 Aged IL-CL=0.0017 CL aged-young>0.9999 IL aged-young>0.9999
7(d) (oligodendrocyte)	12 cells (young) 12 cells (aged) from 4 mice per group	Normal distribution	One-way ANOVA; Bonferroni *post hoc*	$F_{(3, 44)} = 5.552$	ANOVA P=0.0025 Young IL-CL=0.0189 Aged IL-CL=0.1063 CL aged-young>0.9999 IL aged-young>0.9999
7(f) (neuron)	20 cells (young) 20 cells (aged) from 4 mice per group	Normal distribution	One-way ANOVA; Bonferroni *post hoc*	$F_{(3, 76)} = 23.88$	ANOVA P<0.0001 Young IL-CL=0.0048 Aged IL-CL<0.0001 CL aged-young>0.9999 IL aged-young=0.0108
7(f) (astrocyte)	20 cells (young) 20 cells (aged) from 4 mice per group	Normal distribution	One-way ANOVA; Bonferroni *post hoc*	$F_{(3, 76)} = 1.771$	ANOVA P=0.1598 Young IL-CL=0.3061 Aged IL-CL>0.9999 CL aged-young>0.9999 IL aged-young=0.3061
7(f) (oligodendrocyte)	20 cells (young) 20 cells (aged) from 4 mice per group	Normal distribution	One-way ANOVA; Bonferroni *post hoc*	$F_{(3, 76)} = 66.08$	ANOVA P<0.0001 Young IL-CL=0.0031 Aged IL-CL<0.0001 CL aged-young<0.0001 IL aged-young>0.9999
7(i)	100 cells (young) 100 cells (aged) from 4 mice per group	Normal distribution	One-way ANOVA; Bonferroni *post hoc*	$F_{(3, 396)} = 84.38$	ANOVA P<0.0001 Young IL-CL<0.0001 Aged IL-CL=0.5245 CL aged-young>0.9999 IL aged-young<0.0001

Supplementary Table 2. Differentially expressed genes in microglia from aged mice versus young adult mice after sham operation.

Supplementary Table 3. Functional enrichment results of upregulated DEGs in aged microglia versus young microglia after sham operation.

Supplementary Table 4. Differentially expressed genes in microglia after dMCAO versus sham operation in young adult mice.

Supplementary Table 5. Differentially expressed genes in microglia after dMCAO versus sham operation in aged mice.

Supplementary Table 6. Functional enrichment results of all DEGs in microglia from dMCAO brain versus sham brain in young adult mice.

Supplementary Table 7. Functional enrichment results of all DEGs in microglia from dMCAO brain versus sham brain in aged mice.

Supplementary References

1. National Research Council. *Guide for the Care and Use of Laboratory Animals*. 8th ed. Washington, DC: National Academies Press, 2011.

2. Kilkenny C, Browne WJ, Cuthill IC, et al. Improving bioscience research reporting: the ARRIVE guidelines for reporting animal research. *PLoS Biol* 2010; 8: e1000412.

3. Suenaga J, Hu X, Pu H, et al. White matter injury and microglia/macrophage polarization are strongly linked with age-related long-term deficits in neurological function after stroke. *Exp Neurol* 2015; 272: 109-119.

4. Pu H, Shi Y, Zhang L, et al. Protease-independent action of tissue plasminogen activator in brain plasticity and neurological recovery after ischemic stroke. *Proc Natl Acad Sci U S A* 2019; 116: 9115-9124.

5. Shi Y, Jiang X, Zhang L, et al. Endothelium-targeted overexpression of heat shock protein 27 ameliorates blood-brain barrier disruption after ischemic brain injury. *Proc Natl Acad Sci U S A* 2017; 114: E1243-E1252.

6. Fisher M, Feuerstein G, Howells DW, et al. Update of the stroke therapy academic industry roundtable preclinical recommendations. *Stroke* 2009; 40: 2244-2250.

7. Zhao J, Mu H, Liu L, et al. Transient selective brain cooling confers neurovascular and functional protection from acute to chronic stages of ischemia/reperfusion brain injury. *J Cereb Blood Flow Metab* 2019; 39: 1215-1231.

8. Wang R, Liu Y, Ye Q, et al. RNA sequencing reveals novel macrophage transcriptome favoring neurovascular plasticity after ischemic stroke. *J Cereb Blood Flow Metab* 2020; 40: 720-738.

9. Kim D, Pertea G, Trapnell C, et al. TopHat2: accurate alignment of transcriptomes in the presence of insertions, deletions and gene fusions. *Genome Biol* 2013; 14: R36.

10. Frankish A, Diekhans M, Ferreira AM, et al. GENCODE reference annotation for the human and mouse genomes. *Nucleic Acids Res* 2019; 47: D766-D773.

11. Trapnell C, Williams BA, Pertea G, et al. Transcript assembly and quantification by RNA-Seq reveals unannotated transcripts and isoform switching during cell differentiation. *Nat Biotechnol* 2010; 28: 511-515.

12. Anders S, Pyl PT and Huber W. HTSeq--a Python framework to work with high-throughput sequencing data. *Bioinformatics* 2015; 31: 166-169.

13. R Core Team. R: A language and environment for statistical computing. Vienna, Austria: R Foundation for Statistical Computing, 2018.

14. Robinson MD, McCarthy DJ and Smyth GK. edgeR: a Bioconductor package for differential expression analysis of digital gene expression data. *Bioinformatics* 2010; 26: 139-140.

15. Zhou Y, Zhou B, Pache L, et al. Metascape provides a biologist-oriented resource for the analysis of systems-level datasets. *Nat Commun* 2019; 10: 1523.

16. Walter W, Sanchez-Cabo F and Ricote M. GOplot: an R package for visually combining expression data with functional analysis. *Bioinformatics* 2015; 31: 2912-2914.

17. Kramer A, Green J, Pollard J, Jr., et al. Causal analysis approaches in Ingenuity Pathway Analysis. *Bioinformatics* 2014; 30: 523-530.

18. Zhang W, Zhao J, Wang R, et al. Macrophages reprogram after ischemic stroke and promote efferocytosis and inflammation resolution in the mouse brain. *CNS Neurosci Ther* 2019; 25: 1329-1342.